



## RESEARCH ARTICLE

# Hurricanes enhance coral connectivity but also superspread coral diseases

Thomas Dobbelaere<sup>1</sup>  | Apolline Dekens<sup>2</sup> | Antoine Saint-Amand<sup>1</sup> | Lauranne Alaerts<sup>1</sup> | Daniel M. Holstein<sup>3</sup>  | Emmanuel Hanert<sup>1,4</sup>

<sup>1</sup>Earth and Life Institute (ELI), UCLouvain, Louvain-la-Neuve, Belgium

<sup>2</sup>Ecole Normale Supérieure de Paris (ENS), Paris, France

<sup>3</sup>Department of Oceanography and Coastal Sciences, College of the Coast and Environment, Louisiana State University, Baton Rouge, Louisiana, USA

<sup>4</sup>Institute of Mechanics, Materials and Civil Engineering (IMMC), UCLouvain, Louvain-la-Neuve, Belgium

## Correspondence

Thomas Dobbelaere, Earth and Life Institute (ELI), UCLouvain, Louvain-la-Neuve, Belgium.

Email: [thomas.dobbelaere@uclouvain.be](mailto:thomas.dobbelaere@uclouvain.be)

## Abstract

Climate change poses an existential threat to coral reefs. A warmer and more acidic ocean weakens coral ecosystems and increases the intensity of hurricanes. The wind–wave–current interactions during a hurricane deeply change the ocean circulation patterns and hence potentially affect the dispersal of coral larvae and coral disease agents. Here, we modeled the impact of major hurricane Irma (September 2017) on coral larval and stony coral tissue loss disease (SCTLD) connectivity in Florida's Coral Reef. We coupled high-resolution coastal ocean circulation and wave models to simulate the dispersal of virtual coral larvae and disease agents between thousands of reefs. While being a brief event, our results suggest the passage of hurricane Irma strongly increased the probability of long-distance exchanges while reducing larval supply. It created new connections that could promote coral resilience but also probably accelerated the spread of SCTLD by about a month. As they become more intense, hurricanes' double-edged effect will become increasingly pronounced, contributing to increased variability in transport patterns and an accelerated rate of change within coral reef ecosystems.

## KEYWORDS

biophysical modeling, coral connectivity, Florida's Coral Reef, hurricanes, long-distance dispersal, stony coral tissue loss disease

## 1 | INTRODUCTION

Coral reefs constitute one of the most biologically diverse ecosystems on Earth. While covering only about 0.2% of the ocean floor, they support more than a quarter of all marine life, providing shelter, food, and breeding areas through their complex calcium skeleton (Lyons et al., 2024; Moberg & Folke, 1999; Rogers et al., 2014). Moreover, due to their location in coastal waters and sturdy structure, they act as a protective barrier for coastal areas, absorbing up to 97% of wave energy, reducing coastal erosion and providing critical protection from storms and floods (Elliff & Silva, 2017; Ferrario et al., 2014). Besides their protective qualities, reefs also have a significant economic value through fisheries and tourism, representing an important source of food and protein for coastal communities

that comprise hundreds of millions of people worldwide (Hoegh-Guldberg et al., 2019). Despite their importance for both human and marine life, coral reefs are, however, severely declining worldwide, with ~50% loss in live coral cover since the 1950s (Eddy et al., 2021). This is mostly due to global anthropogenic stressors, such as ocean warming and acidification, and local anthropogenic stressors, such as water pollution, overfishing, and unsustainable coastal development (Bruno et al., 2003; De'ath et al., 2012; Dove et al., 2020).

The Caribbean region has suffered an important coral cover decrease, from ~30% in the 1970s to only ~5% stony coral cover remaining at the beginning of the 2010s (Porter & Meier, 1992; Ruzicka et al., 2013). In Florida, coral cover dropped below 1% in Southeast Florida and to about 6% in the Florida Keys (Grove et al., 2022). This decline was partly due to a succession of disease outbreaks, whose

mortality can be exacerbated by thermal stress (Muller et al., 2018; Muller & van Woesik, 2012). In the 1970s and 1980s, white band disease decimated nearly 80% of the Acroporid species, the dominant species in the Caribbean region (Aronson et al., 2001; Kline & Vollmer, 2011). Since 2014, stony coral tissue loss disease (SCTLD) has struck the southeastern Florida region and has then spread to the majority of the Caribbean area (Precht et al., 2016). It has affected more than 20 species of corals and shown high mortality rates (Alvarez-Filip et al., 2022). Once a coral shows signs of the disease, the entire colony will likely die within weeks to months (NOAA, 2020).

Global warming also increases the intensity of extreme weather events such as tropical cyclones (also known as typhoons or hurricanes) (Bhatia et al., 2019; Knutson et al., 2020), which can be both beneficial and detrimental to coral reefs. The large waves produced by hurricanes can cause coral branches to break, colonies to dislodge, and hence damage the whole reef framework (Carter et al., 2022; Scoffin, 1993). However, with the reproductive process known as fragmentation, this situation can occasionally be beneficial for coral colonies (Bonin et al., 2011). If the separated coral fragments manage to reattach to the sea floor, they can potentially start a new colony of their own. Storm surges can also damage coastal buildings and shift sands, which can lead to the release and resuspension of sediments that increase the water turbidity and can smother corals, hence preventing their symbiotic algae from photosynthesizing (Ertfemeijer et al., 2012; Jones et al., 2015). Furthermore, hurricanes can increase coral stress by driving large volumes of fresh water into the ocean and mixing the water column (Allahdadi & Li, 2017). This causes a sudden decrease in salinity and changes the surface water composition, disturbing coral colonies. Nevertheless, by cooling the sea surface and through local upwelling, which brings deeper and cooler water to the surface, hurricanes can alleviate thermal stress on coral reefs, which can reduce the severity of bleaching and help coral recovery, thus mitigating some impacts of global warming (Aijaz et al., 2017; Carrigan & Puotinen, 2014; Manzello et al., 2007; Varlas et al., 2020).

High wind and wave-induced currents generated by hurricanes also strongly impact the ocean transport processes (Dobbelaere, Curcic, et al., 2022; Liu et al., 2020; Oey et al., 2007). This is particularly true for larval dispersal and thus for coral connectivity, as coral larvae are transported by oceanic currents before settling upon a reef (Shulman & Bermingham, 1995). On the one hand, the passage of a hurricane can modify larval dispersal pathways leaving some reefs more isolated and thus more vulnerable to disturbances (Grimaldi et al., 2022). On the other hand, the change in larval dispersal can promote coral gene exchanges by creating new connections between otherwise disconnected reefs, which in turn increases the genetic diversity and robustness of the entire system. For instance, Radford et al. (2014) showed that cyclones had the potential to connect widely separated reefs of the North West Shelf of Australia by increasing the distance larvae travel. However, since some coral disease agents may also be transported by currents (Dobbelaere et al., 2020), the passage of a hurricane could also accelerate the propagation of a disease, allowing it to reach reefs that would not have been affected otherwise. The impact of hurricanes on coral reef connectivity thus presents a

complex dynamic, simultaneously enhancing and inhibiting the resilience of coral reefs on multiple scales.

Here, our objective was to disentangle those two opposing effects by considering the passage of a major hurricane through a dense reef system during the coral spawning season. We consider hurricane Irma, which made landfall in Florida on September 10, 2017, as one of the most intense hurricanes to cross Florida's Coral Reef (FCR). It struck during the reproduction period of several reef-building coral species (Bright et al., 2021a), but also while Florida reefs were being exposed to SCTLD. More specifically, our objectives are (1) to assess the effect of hurricane Irma on coral connectivity in FCR and (2) to determine whether hurricane Irma may have acted as a superspreader event for SCTLD.

To achieve these objectives, we coupled the multiscale coastal ocean model SLIM<sup>1</sup> (Frys et al., 2020; Lambrechts et al., 2008) with the spectral wave model SWAN<sup>2</sup> (Booij et al., 1999; Dobbelaere, Curcic, et al., 2022) to represent wind-wave-current interactions induced by the hurricane. We used the modeled ocean currents and wave-induced Stokes drift velocities to simulate the dispersal of both coral larvae and SCTLD disease agents between the thousands of reefs composing FCR. We compared the coral and disease dispersal patterns initiated before the passage of the hurricane to those initiated just after. Exchanges of coral larvae and disease agents between reefs yield potential connectivity matrices that were analyzed with graph-theory algorithms to identify the main changes induced by the hurricane and their impact on the connectivity metrics. Finally, we simulated the disease propagation between September 1, 2017, and December 1, 2017, using a connectivity-based epidemiological model (Dobbelaere et al., 2020) to quantify the hurricane-induced acceleration of the epidemics front.

## 2 | MATERIALS AND METHODS

### 2.1 | Study area

Florida's Coral Reef is the third largest barrier reef in the world (Finkl & Andrews, 2008). It extends over 580 km along the southern and eastern coasts of Florida, just north of the Florida Strait that connects the Gulf of Mexico to the Atlantic Ocean. FCR is home to almost 1400 marine species, including more than 40 species of stony corals (Banks et al., 2008). The southern part of FCR is known as the Keys. It is an archipelago of limestone islands, which stretches from the southeastern coast of the Florida peninsula to the Dry Tortugas National Park (DRTO). The Florida Keys include, from west to east, the DRTO, which is the most isolated part of FCR, the Marquesas Keys, the Lower Keys, and the Middle and Upper Keys, which are exposed portions of an ancient coral reef (Figure 1a). The northern

<sup>1</sup>Second-generation Louvain-la-Neuve Ice-ocean Model (SLIM, <https://www.slim-ocean.be>).

<sup>2</sup>Simulating WAVes Nearshore (SWAN, <https://swanmodel.sourceforge.io>).

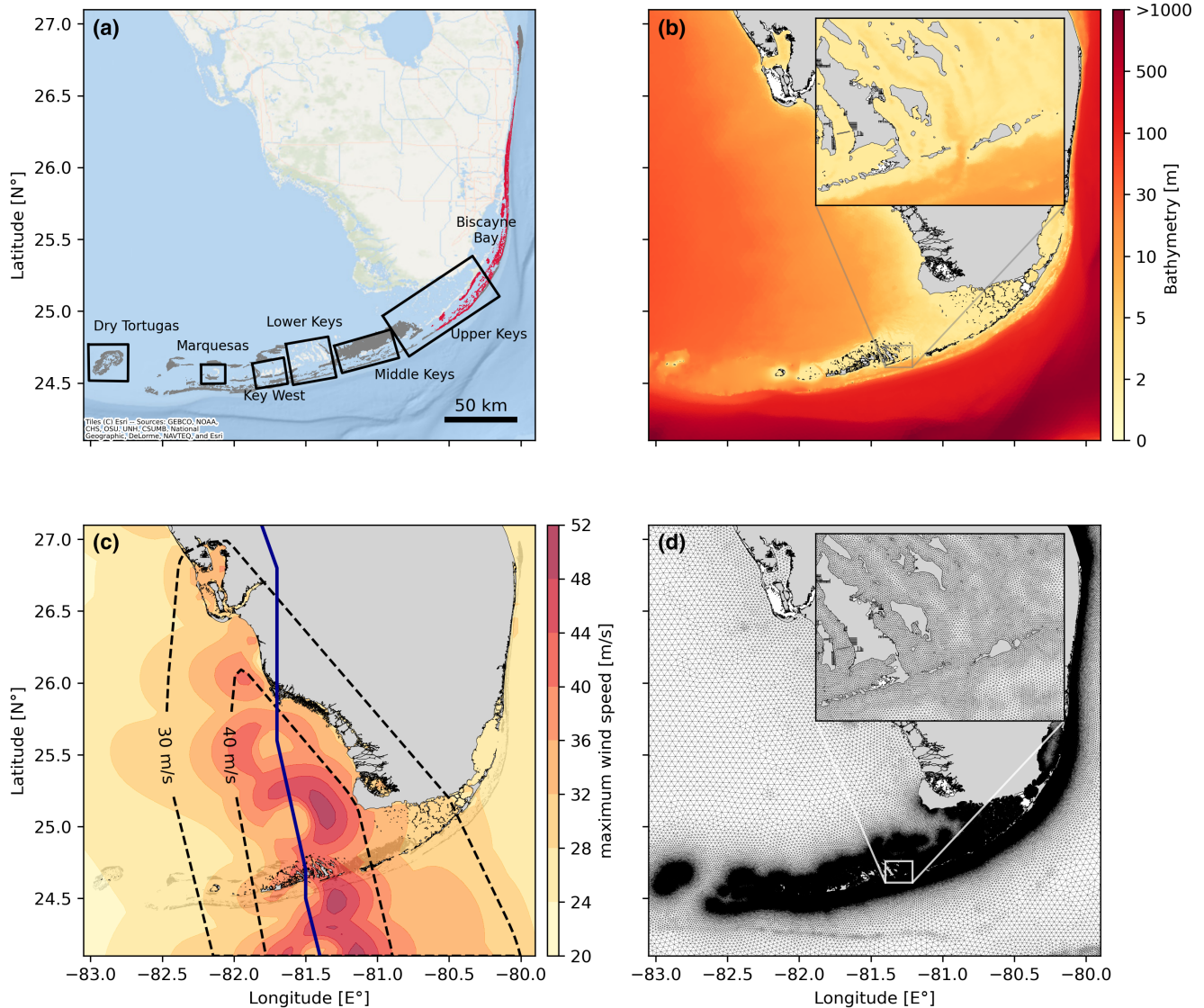


**FIGURE 1** Overview of the area of interest with (a) Florida's Coral Reef (FCR) with healthy/susceptible reefs shown in dark gray and infected reefs shown in red, (b) the model bathymetry, (c) the maximum wind speed during Hurricane Irma (30 and 40 m/s isolines in black dotted lines and track of Irma in dark blue), and (d) the model unstructured mesh whose resolution ranges from ~100m near the coast and reefs in FCR to ~5km offshore.

extension of FCR, the Southeast Florida Reef Tract, consists of relict reefs with rather low living hard coral cover (Banks et al., 2008; Hoffmeister & Multer, 1968).

The ocean circulation in FCR is dominated by the Florida Current (FC), which flows eastward through the Florida Strait. It originates from the Loop Current, a warm fast-moving current flowing between the Yucatan peninsula and Cuba in the Gulf of Mexico, and then follows the eastern coast northward to join the Gulf Stream. Coral reefs were able to thrive in the Florida Keys thanks to the warm waters from the Loop Current (Donahue et al., 2008). Occasionally, an anticyclonic eddy separates from the Loop Current, subsequently changing the position of the FC and causing it to meander along FCR (Leipper, 1970; Vukovich, 1988). The interaction between the meandering flow and the topography of FCR generates cyclonic eddies throughout FCR (Kourafalou &

Kang, 2012). These eddies have a significant impact on coral connectivity by creating new connectivity pathways (Limouzy-Paris et al., 1997) and increasing larval retention on the southwest shelf (Lee et al., 1994). On the other hand, on the inner West Florida shelf and in the nearshore region, water circulation is predominantly governed by local winds and tides (Lee & Smith, 2002; Sponaugle & Lee, 2007).

Florida is often affected by hurricanes and tropical storms. The hurricane season usually runs from June to November, when the Atlantic Ocean is the warmest (Neumann, 1999). On average, Florida is hit by a hurricane once every 2 years and once every 4 years by major hurricanes, with the southern coast being especially affected (Her et al., 2021; Malmstadt et al., 2009). Hurricane Irma, which struck Florida in September 2017, was one of the most intense and destructive hurricanes on record in the Atlantic Basin (Cangialosi

et al., 2018; Xian et al., 2018). Irma started as a tropical wave near the Cape Verde islands on August 27, 2017, and rapidly developed into a Category 3 hurricane by August 31, peaking as a Category 5 hurricane on September 6, near Barbuda island. It made landfall in the Florida Keys on September 10 at 1 p.m. UTC as a Category 4 hurricane, with winds reaching 213 km/h (Figure 1c), and then weakened after reaching mainland Florida as it moved further inland, ultimately dissipating over Missouri on September 13.

The passage of Hurricane Irma inflicted substantial damage on Florida. In the Florida Keys, 65% of buildings sustained severe damage, with 25% completely destroyed, leading to a total of \$50 billion in property damage. This rendered Irma one of the most destructive and costly hurricanes in the history of the Atlantic Basin (Cangialosi et al., 2018; NOAA, 2018a). The coral reefs, particularly those located south of Irma's landfall in the Florida Keys, suffered extensive damage, including fractures, abrasions, lesions, and suffocation, leading to widespread coral mortality. High levels of sponge mortality were also observed in certain locations (NOAA, 2022).

## 2.2 | Coupled wave-current model

We simulated ocean circulation during Irma using the high-resolution coupled wave-current model SLIM+SWAN developed and validated during Hurricane Irma by Dobbelaere, Curcic, et al. (2022). In this coupled model, ocean current are simulated using the 2D barotropic mode of the unstructured-grid multiscale ocean model SLIM, which solves the conservative form of the shallow water equations:

$$\frac{\partial H}{\partial t} + \nabla \cdot (\mathbf{U}) = 0, \quad (1)$$

$$\frac{\partial \mathbf{U}}{\partial t} + \nabla \cdot \left( \frac{\mathbf{U}\mathbf{U}}{H} \right) + f\mathbf{e}_z \times \mathbf{U} = gH\nabla(H-h) - \frac{H}{\rho} \nabla p_{\text{atm}} + \frac{1}{\rho} \tau_s + \nabla \cdot (\nu \nabla \mathbf{U}) - \frac{C_b}{H^2} |\mathbf{U}| \mathbf{U} + \gamma (\mathbf{U}_{\text{ref}} - \mathbf{U}), \quad (2)$$

where  $H$  is the water column height and  $\mathbf{U}$  is the depth-averaged transport;  $f$  is the Coriolis coefficient;  $g$  is the gravitational acceleration;  $h$  is the bathymetry;  $\nu$  is the Smagorinsky viscosity;  $C_b$  is the bulk bottom drag coefficient;  $p_{\text{atm}}$  is the atmospheric pressure;  $\tau_s = \tau_s^{\text{wind}} + \tau_s^{\text{waves}}$  is the surface stress due to wind and waves. To withstand potential drying in parts of the model grid during the hurricane, these equations were solved using a wetting-drying algorithm (Le et al., 2020). As most coral reefs are located at depth shallower than 20 m, 2D unstructured-grid models are able to accurately simulate the barotropic dynamics prevailing in shallow areas while allowing for a 100-m spatial resolution over reefs at a tractable computational cost. Furthermore, barotropic phenomena were indirectly captured by gradually relaxing the simulated transport toward a reference transport  $\mathbf{U}_{\text{ref}}$  with coefficient  $\gamma$  in regions where water depth was exceeding 50 m. This reference transport was obtained by depth integration of the velocity field produced by the operational model HYCOM (Chassignet et al., 2007). This allowed the model to indirectly represent the mesoscale eddies occurring along the FC or south of FCR (Frys et al., 2020).

The wave component of the coupled model is the unstructured parallel version of the spectral wave model SWAN, which solves the action balance equation:

$$\frac{\partial N}{\partial t} + \nabla_{\mathbf{x}} \cdot [(\mathbf{c}_g + \mathbf{u})N] + \frac{\partial}{\partial \theta} [c_\theta N] + \frac{\partial}{\partial \sigma} [c_\sigma N] = \frac{S_{\text{in}} + S_{\text{ds}} + S_{\text{nl}}}{\sigma}, \quad (3)$$

where  $N$  is the wave action density;  $\theta$  is the wave propagation direction;  $\sigma$  is the intrinsic wave frequency;  $\mathbf{c}_g$  is the wave group velocity,  $\mathbf{u} = \mathbf{U}/H$  is SLIM depth-averaged current velocity;  $c_\theta$  and  $c_\sigma$  are the propagation velocities in spectral space due to refraction and shifting in frequency due to variations in depth and currents; and  $S_{\text{in}}$ ,  $S_{\text{ds}}$ , and  $S_{\text{nl}}$  respectively represent wave growth by wind, wave decay and nonlinear transfers of wave energy through four and three-wave interactions, that is, quadruplets and triplets. The wave and current components were coupled through the radiation stress gradient  $\tau_s^{\text{waves}}$ , that is, the force exerted by waves on currents, computed by SWAN and accounted for in Equation (2). Moreover, the modeled wave energy spectra were used to compute the Stokes drift, that is, the net drift in the direction of the wave propagation, as in Dobbelaere, Curcic, et al. (2022). This wave-induced transport was used in combination with SLIM's depth-averaged current velocity to simulate the dispersal of coral larvae and disease agents.

The model bathymetry (Figure 1b) was built by combining three data sources: the General Bathymetric Chart of the Ocean (GEBCO; 15 arc-seconds resolution), the Coastal Relief Model (NOAA National Geophysical Data Center, 2001; 3 arc-seconds resolution), and NOAA's bathymetric Digital Elevation Model (National Centers for Environmental Information, 2018; 1/3 arc-seconds resolution). Hurricane Irma's wind field (Figure 1c) was reconstructed using high-resolution H\*Wind wind fields (Powell et al., 1998). However, as H\*Wind wind profiles did not cover the entirety of our domain, we combined it with a coarser wind field extracted from the European Centre for Medium-Range Weather Forecasts (ECMWF) ERA-5 dataset (Hersbach et al., 2020). The pressure field during the passage of Irma was reproduced by merging ERA-5 data, for the baseline pressure field, with an idealized Holland pressure profile for the central depression (Dobbelaere, Curcic, et al., 2022). The tidal forcing data were recovered thanks to the OSU TOPEX/Poseidon Global Inverse Solution dataset (Egbert & Erofeeva, 2002). The coupled wave-current model equations were solved on an unstructured triangular mesh (Figure 1d), whose resolution varies according to the bathymetry and distance to coast and to the reefs. It is composed of about  $7 \times 10^5$  elements and its resolution ranges from approximately 100 m in FCR to 5 km offshore. The ocean circulation and wave models have been thoroughly validated on FCR with respect to ocean currents, sea surface elevation and significant wave height observations (Dobbelaere, Curcic, et al., 2022; Dobbelaere, Holstein, et al., 2022; Frys et al., 2020). Additional validation results for the currents during September 2017 are provided in Appendix.

We simulated the ocean currents from August 1, 2017, to January 1, 2018, and wind-generated waves from September 5 to 15, 2017, to consider the hydrodynamic conditions prevailing before and after the passage of the hurricane. The simulated ocean

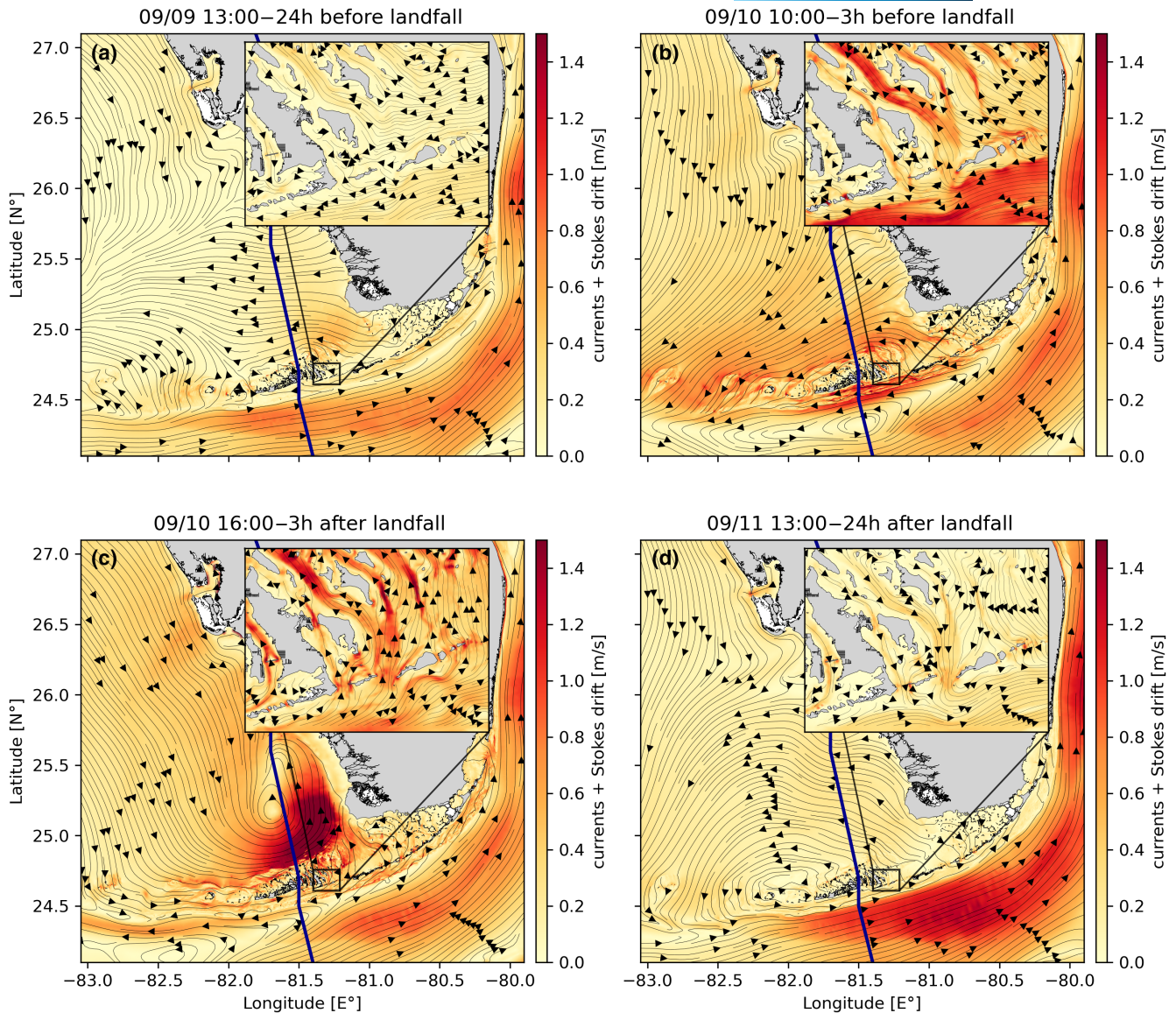


**FIGURE 2** Snapshots of the combined modeled depth-averaged currents and Stokes drift (a) 24h before landfall, (b) 3h before landfall, (c) 3h after landfall, and (d) 24h after landfall. Note that strong westward current developing offshore of the Lower Keys in panel (b). The trajectory of the hurricane is depicted by a solid blue line.

currents and waves Stokes drift are combined to form a transport velocity that will drive the dispersal of coral larvae and disease agents (Figure 2). In fair-weather conditions, the Stokes drift is usually negligible compared to the ocean currents (Dobbelaere, Curcic, et al., 2022), and it should hence be taken into account to simulate transport processes. One day before and after the passage of the hurricane, the combined ocean currents and Stokes drift show the usual flow patterns in FCR, which is dominated by the FC acting as a strong northeastward conveyor belt. The flow through the Lower Keys reef system and on the inner shelf is weak (Figure 2a,d). In the hours preceding Irma's landfall in the Keys, the transport velocity becomes much more intense just offshore of the Lower Keys leading to a reversal of the transport dynamics westward with current speeds exceeding 1 m/s. The flow through the

reef system is also much more intense (>1 m/s) and directed northward (Figure 2b). After landfall, the transport velocity intensifies on the inner shelf and keeps on accelerating the flow through the Lower Keys. Offshore of the Keys, the flow starts to weaken and the eddy that led to the westward flow intensification moves west (Figure 2d).

### 2.3 | Transport model

The simulated depth-averaged currents and Stokes drift were used to model the dispersal of both coral larvae and disease agents throughout FCR using a Lagrangian biophysical model. Coral spawning of several reef building species found in FCR have been reported to take place 7–10 days following a full moon in August or September (Hagman et al., 1998). More specifically, spawning of *Montastrea*

*cavernosa* has already been observed during nights 6–8 after the September full moon in the region of Miami (Bright et al., 2021). Based on the full moon of September 2017, it was expected to spawn on the nights of September 12–14. Given the proximity of possible *M. cavernosa* spawning times with the passage of Irma, we simulated the dispersal of larvae originating from two hypothetical spawning events, one occurring three nights before the passage of Irma (on September 7–9) and one occurring three nights just after its passage (on September 10–12).

The biophysical model represents larval mortality, acquisition and loss of competence, and settlement behaviors. These behaviors were parameterized as in Frys et al. (2020), based on laboratory measurements from Kuba (2016). For *M. cavernosa*, it takes approximately 3.8 days for larvae to become competent after they have been spawned and hence acquire the ability to alter their buoyancy and settle on a reef. However, after a certain period, they exhaust their energy reserves, thereby losing this ability to settle on a reef. The competency acquisition and loss rates were set at 6.4% and 1.6% per day, respectively (Kuba, 2016). In addition, larvae may perish before reaching a reef to settle on. Larval mortality was modeled as a fixed daily probability of dying. It was set at a rate of 6.7% per day, such that the average larval life expectancy was approximately 15 days (Kuba, 2016). When competent larvae are over a reef, we assume they can settle at a rate 20% per hour based on larval vertical swimming speed, as in King et al. (2023).

Finally, once all the necessary parameters were set, virtual particles were released on all FCR reefs. The reef shapefile used to locate the different reefs in FCR was extracted from the “coral reefs and hardbottom” layer of the Unified Florida Reef Tract Map (Florida Fish and Wildlife Conservation Commission–Fish and Wildlife Research Institute, 2017). The polygons representing the reefs were then divided into 500 m × 500 m sub-reefs, amounting to 16,823 sub-reefs. This subdivisions was performed in Dobbelaere et al. (2020) in order to capture the dynamics of the propagation of SCTLD within the reefs at a scale consistent with the model resolution, as the original polygons varied in width, shape and area, and could reach several kilometers in size. For each larval dispersal simulation, we seeded particles every 450 s from 15 to 225 min after sunset and released in total 820 particles/km<sup>2</sup>, which is much higher than the particle density threshold required to get connectivity results independent of the number of particles released (Monroy et al., 2017). The dispersal simulations following both spawning events had a duration of 3 months. Although coral density observations are available, their spatial resolution is too coarse to be used in our model. Consequently, we only modeled potential connectivity and assumed that all the reefs had the same *M. cavernosa* coral cover and were all suitable for larval settlement, which is not the case in reality. However, as the purpose of this study was only to compare the potential connectivity with and without the hurricane, this assumption is acceptable.

For the disease agents, we considered a simulation starting on September 5 00:00 UTC and for which particles were released every 4 h during 3 days with a density of 100 particles/km<sup>2</sup> ( $\sim 2.6 \times 10^6$

particles in total). This allowed us to represent a situation where disease agents were already present in the water in the entire area where the disease was present before Irma. Disease agents were only released on reefs where the disease signs were observed prior to September 2017. The position of the disease front was estimated by spatially interpolating the time of disease observation by kriging with a Gaussian semivariogram using Python pyKrig module (Murphy, 2014), as in Dobbelaere et al. (2020). Disease observations were compiled from the seven datasets used in Muller et al. (2020): (i) Coral Reef Evaluation and Monitoring Project (CREMP; 2014–2017), (ii) CREMP Presence/Absence Data (CREMP P\_A; 2016–2017), (iii) Southeast Florida Coral Reef Evaluation and Monitoring Project (SECREMP; 2014–2017), (iv) Florida Reef Resilience Program Disturbance Response Monitoring (FRRP; 2014–2017), (v) Hurricane Irma Rapid Reef Assessment [IRMA; 2017; (Viehman et al., 2018)], (vi) the Southeast Florida Action Network citizen science program (SEAFAN; 2014–2017), and (vii) the Southern Coral Disease Margin field effort [2017 and 2018; (Neely, 2018)]. It is important to note that no case definition of the visual appearance and ecology of SCTLD was available before 2018 (NOAA, 2018b). The datasets that we used could thus contain observations of tissue loss consistent with SCTLD but corresponding to another disease, such as the white plague coral disease. The other simulation started on September 12 00:00 UTC and also involved the release of particles during 3 days at the same rate. Disease agents were assumed to be transported within composite material (like dying tissue or resuspended sediments) mixed within the water column and hence driven by the barotropic currents. They were further assumed to have a half-life of 30 days to account for the decay of the agent vector in the water column. These properties were chosen as they allowed to accurately reproduce the observed spread of SCTLD in FCR in 2018–2019 in a previous study (Dobbelaere et al., 2020).

## 2.4 | Connectivity indicators

The biophysical model simulations yield  $16,823 \times 16,823$  connectivity matrices, denoted  $C$  with entries  $C_{ij}$ . They represent the mass of particles released on sub-reef  $i$  that settled on sub-reef  $j$ . It can be normalized by dividing each row by the number of particles released on the corresponding sub-reef to obtain the normalized connectivity matrix  $\tilde{C}$ . As such large matrices are very hard to analyze, we use instead graph theory tools to extract ecologically meaningful connectivity indicators (Figueiredo et al., 2022; Frys et al., 2020; Thomas et al., 2014). We hence interpret the connectivity matrices as large directed graphs whose vertices represent reefs and edges correspond to non-zero entries in the matrix. The different connectivity indicators used in this study are defined in Table 1. These are standard connectivity measures indicating the average dispersal distance or weighted connectivity length (WCL), the fraction of particles released that settles somewhere ( $P^{\text{settled}}$ ), the potential to provide many particles to many reefs (OC), and the potential to receive many particles from many different reefs (IC).

**TABLE 1** Connectivity indicators used to analyze the dispersal of coral larvae and disease agents in the reef network.

Indicator	Formula	Description
Weighted connectivity length	$WCL_i = \frac{\sum_j \tilde{C}_{ij} L_{ij}}{\sum_j \tilde{C}_{ij}}$	Average dispersal distance from origin to destination reef for all particles released over a reef
Proportion settled	$p_i^{\text{settled}} = \sum_j \tilde{C}_{ij}$	Proportion of particles released by a reef that manage to settle
Outgoing connectivity	$OC_i = N_i^{\text{out}} \sum_j \tilde{C}_{ij}$	Number of outgoing connections originating from a given reef multiplied by the total mass of particles originating from this reef that settled on a reef
Incoming connectivity	$IC_i = N_i^{\text{in}} \sum_j \tilde{C}_{ji}$	Number of incoming connections pointing to a given reef multiplied by the total mass of particles that settles on that reef

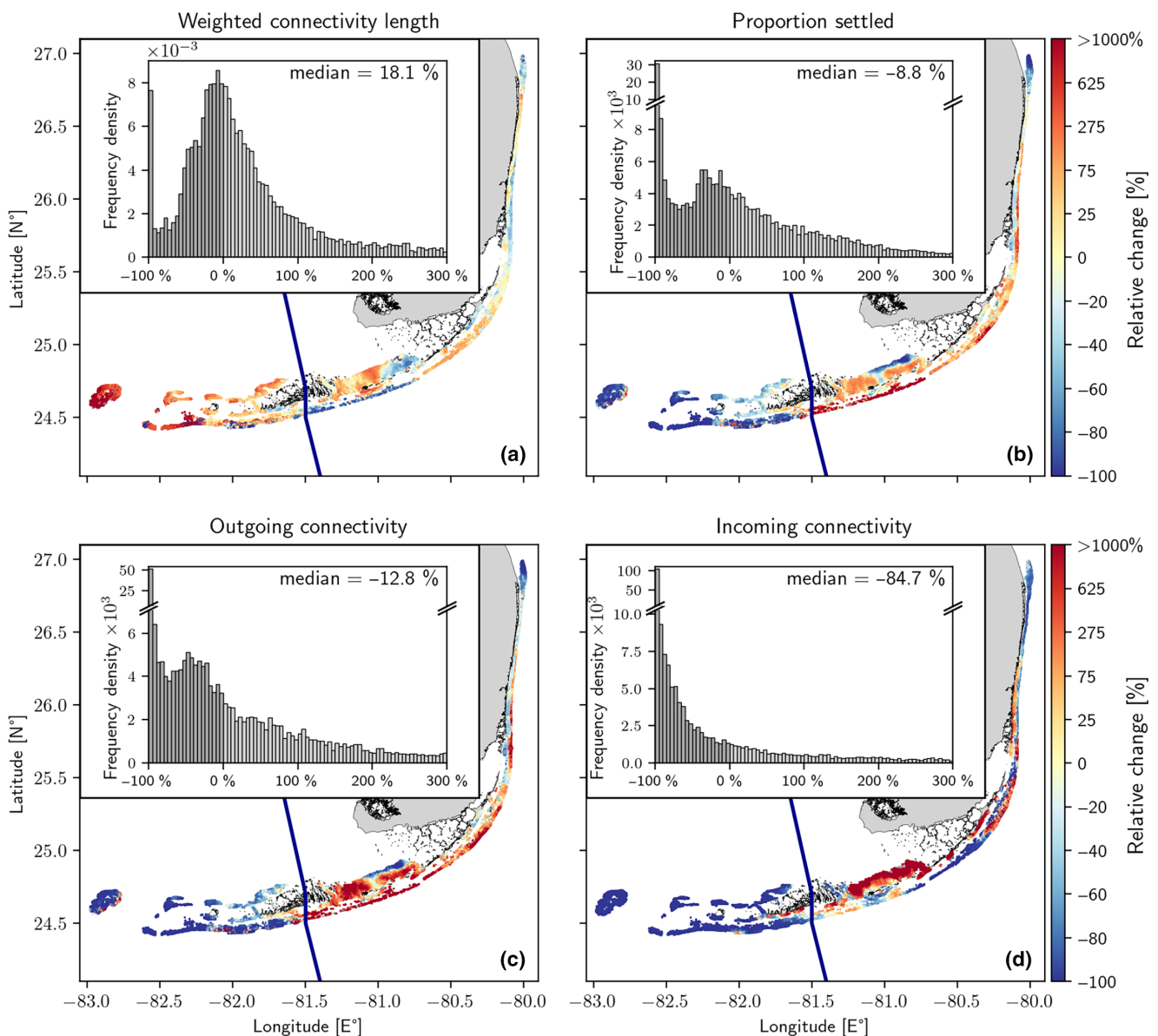


**FIGURE 3** Spatial distributions alongside frequency density histograms illustrating the relative changes induced by Hurricane Irma in larval (a) weighted connectivity length, (b) proportion settled, (c) outgoing connectivity, and (d) incoming connectivity. The trajectory of Hurricane Irma is depicted by a solid blue line. The horizontal axis of the histograms has been cropped to 300% to improve readability.

## 2.5 | Epidemiological model

The connectivity matrices were then used to model disease propagation using the connectivity-based Susceptible-Infectious-Removed (SIR) epidemiological model developed by Dobbelaere et al. (2020). In this model, a uniform density of corals with species-averaged susceptibility to SCTLD is assumed on all sub-reef polygons. The coral populations on these sub-reefs are then further divided into susceptible (S), infectious (I) and removed (R) fractions (i.e.,  $S_i + I_i + R_i = 1$  on every sub-reef  $i$ ). Infection of susceptible corals on a given sub-reef polygon by infectious individuals from another sub-reef polygon is enabled when these reefs are connected in the disease networks and depends on the strength of the connection. Additionally, to account for coral resistance to the disease, infection within the same sub-reef polygon is only activated when the proportion of infectious corals on that sub-reef is greater than a given infection threshold  $I_0$ . Dobbelaere et al. (2020) identified a well-defined range of infection threshold values for which the model accurately reproduced the observed spread of the disease between May 2018 and April 2019.

The disease connectivity matrices from both the hurricane and no-hurricane scenarios were input into the model, and simulations were conducted from September 1, 2017, to December 1, 2017, for various values of  $I_0$  within the range of valid values identified in Dobbelaere et al. (2020). We employed the same calibrated transmission and removal parameters as in Dobbelaere et al. (2020), and the initial conditions of the model were calculated using a simplified SIR model following the methodology of Dobbelaere et al. (2020). Furthermore, the rows and columns corresponding to the so-called *Vaca Reef* (Figure 5, Frys et al., 2020), which is particularly large but with a very low coral cover, were removed from the connectivity matrices to avoid an overestimation of the disease propagation (Dobbelaere et al., 2020). For each simulation, the total infected area and the distance traveled by the disease front were computed.

## 3 | RESULTS

Hurricane Irma's impact on larval and disease connectivity has been assessed by comparing modeled dispersal patterns initiated before and after the passage of the hurricane on September 10 at 9 a.m. EDT (1 p.m. UTC). For coral larvae, we considered two hypothetical spawning events of *M. cavernosa* occurring on September 7–9 and on September 10–12. For the disease, we considered disease agents produced on September 5–7 and on September 12–14. Releasing disease agents earlier allowed us to better represent the situation prevailing during the passage of the hurricane where disease agents were already present in the water in the entire area affected by the disease. All the graphs presented in this section display relative changes computed by comparing larval and disease dispersal simulations impacted by the passage of the hurricane to similar simulations initiated just after its passage. For each connectivity indicator, we present both its relative change spatial distribution and its frequency

density histogram. Since the latter is generally not normally distributed, the description of the results focuses on the median rather than on the mean of the distributions.

### 3.1 | Larval dispersal

The relative changes to the four connectivity indicators clearly highlight a difference in connectivity between reefs located to the west versus to the east of the hurricane's track (Figure 3). While the passage of Irma led to a global increase of the WCL with a median relative change of 18%, this increase is most apparent for the reefs west of the track (Figure 3a). Almost all these reefs saw their WCL substantially increase, with more than 10-fold increases observed for certain reefs, such as those in the Dry Tortugas and south of the Marquesas. Conversely, east of the hurricane track, the variability was more pronounced with alternating patches of WCL increase and decrease present on both the inner and outer shelves.

Model results also show that Irma strongly impacted the proportion of larvae that settles (Figure 3b). While the median of this change is slightly negative (−8.8%), the spatial distribution shows large variations. Reefs situated west of the track predominantly experienced a strong decrease in the proportion of their larvae that settled, suggesting that larvae are transported to areas lacking coral reefs or that their mortality increased as they take longer to settle. In contrast, the offshore reefs located east of the track witnessed a substantial increase in their proportion settled, sometimes exceeding 10-fold. West of the hurricane track and on the Middle Keys' outer shelf, WCL, and proportion settled are inversely correlated as reefs that observed an increase in their WCL generally also witnessed a decrease in their proportion settled and vice versa. This correlation however does not hold further north in the track.

The simulated change in outgoing connectivity exhibits a similar pattern as the change in the proportion settled (Figure 3c). Overall, the median is again negative (−12.8%) but the differences between the reefs are even more striking. A majority of the reefs west of the track witnessed a significant reduction in their source index, particularly for reefs in the Dry Tortugas, near the Marquesas, and on the outer shelf. These are the same reefs for which the increase in WCL was the largest, as was already evident in the proportion settled distribution. East of the track, there are reefs with considerable increases, especially in the Middle Keys and on the outer shelf.

Lastly, the relative change in incoming connectivity underscores that only a few reefs strongly benefited from the shifts in connectivity patterns driven by Irma (Figure 3d). The relative change distribution's median is notably low (−84.7%), indicating that the vast majority of reefs witnessed a decline in their larval supply. Most reefs west of the track and those east of the track on the outer shelf experienced a pronounced decrease, often resulting in a complete disappearance of larval supply. The clear beneficiaries were the inner-shelf reefs in the Middle Keys, reefs in the Upper Keys, and some reefs near the coast north of Biscayne Bay.



### 3.2 | Disease dispersal

As our objective was to determine whether Irma accelerated the spread of SCTLD, we focused only on connections from reefs that were infected at the time of Irma's passage (refer to the distribution in [Figure 1a](#)) to those that were healthy (i.e., susceptible) within the connectivity matrix. Consequently, metrics such as WCL, proportion settled, and outgoing connectivity were calculated only for infected reefs, while incoming connectivity was calculated only for susceptible reefs.

Although the distribution of relative changes in WCL indicates that the majority of infected reefs saw a reduction in the distance over which they could transmit disease agents during the hurricane's passage, some reefs experienced a strong increase in WCL ([Figure 4a](#)). This surge was primarily due to infected reefs in the Upper Keys, which were at the forefront of the SCTLD epidemic in September 2017. Some of these reefs witnessed their WCL more than double in the aftermath of Irma's passage. Conversely, infected reefs further north generally experienced a decrease in their WCL.

Examining the proportion of disease agents that successfully reached a susceptible reef, we notice a pronounced increase of 38.6% in the median of the relative change histogram, suggesting an overall increase for the majority of reefs ([Figure 4b](#)). Infected reefs situated at the frontline of the epidemic, which experienced an increase in their WCL, also witnessed a significant increase in the proportion of disease agents they produce that reached susceptible reefs. Similarly, infected reefs further north, where the WCL decreased, also saw a comparable increase in their proportion settled.

The distribution of the simulated outgoing connectivity indicator reinforces the previous findings ([Figure 4c](#)). It highlights a cluster of infected reefs in the Upper Keys, at the forefront of the epidemic, that underwent a substantial increase in their outgoing connectivity index, often exceeding tenfold. This implies that these infected reefs transmitted more disease agents to a greater number of susceptible reefs due to the passage of the hurricane. On the whole, the median of the frequency density distribution saw a significant increase (+59%), suggesting that the majority of infected reefs became more potent sources of disease, thereby potentially accelerating the progression of the epidemic.

The distribution of incoming connectivity pinpoints which susceptible reefs could have received the most disease agents from the infected reefs ([Figure 4d](#)). Three areas stand out: a large reef cluster on the inner shelf of the Middle Keys, almost contiguous to the disease front, a smaller cluster of reefs on the outer shelf of the Middle Keys, and an even smaller cluster on the outer shelf of the Lower Keys (see arrows in [Figure 4d](#)). The first and last of these areas correspond to substantial increases in incoming disease agents, often exceeding tenfold. This suggests that Irma could have facilitated the disease's spread to reefs far from the disease front and into areas like the inner shelf, which would typically be more challenging for disease agents to reach under normal flow conditions. Overall, it appears that the majority of susceptible reefs experienced an increase

in their exposure to disease agents, with a relative change median of +17.2%.

Finally, we ran epidemiological model simulations with the disease connectivity matrices obtained with and without the hurricane. Model results suggest that the passage of Irma helped the disease to propagate further away and affect more reefs ([Figure 5](#)). It drove the disease agents both shoreward and further westward, causing the disease to spread to reefs near Lower Matecumbe Key instead of reefs directly adjacent to the initial disease front. On average, this "leapfrog" caused a 28.9% increase in propagation distance and an 87.0% increase in affected area compared to the reference simulation. Dividing the difference in disease propagation between the hurricane and reference (i.e., not influenced by Irma) simulations by the disease propagation speed of the reference simulation, we obtain that the impact of the hurricane was equivalent to about 25 days of disease spread under fair weather condition.

The results of our epidemiological model were validated against disease presence and absence observations made after the passage of the hurricane and until December 1, 2017 (see red triangles and black crosses in [Figure 5](#)). By mid-October, SCTLD lesions were observed at three sites ahead of the disease front location before the hurricane. One of these disease observations is rather close to the initial front position and on a reef that was not predicted to be infected when taking Irma into account. However, the two other sites correspond to reefs at the forefront of the area that we identified as potentially infected by long-distance disease agents dispersal driven by the hurricane. Although our model tends to overestimate the area affected by the disease on inshore reefs, the position of the disease front at the end of the simulation is better reproduced using the connectivity matrices impacted by Irma. Without Irma, the modeled disease front on December 1, 2017, was located about 12km east of the locations where disease signs were reported in mid-October 2017. This supports the idea that the passage of Irma accelerated the spread of the SCTLD epidemic.

## 4 | DISCUSSION AND CONCLUSIONS

By taking Hurricane Irma as a test case, our study illustrates how major hurricanes' impact on connectivity can be a double-edged sword; they promote genetic mixing among coral reefs, can foster the recolonization of remote areas and facilitate range expansion but they can also accelerate the spread of coral diseases. The main consequences of a hurricane on the hydrodynamics are wind-wave-current interactions that intensify and deflect the usual transport pathways. As a result, both coral larvae and coral disease agents can be transported further away and reach reefs they may not normally reach. In the case of the SCTLD epidemic, which had already covered about half of FCR at the time of Irma's passage, it was able to advance over a distance that would typically take about a month to be covered under fair weather conditions. However, at the same time, larval exchanges between separated coral reefs became longer, with half of all reefs experiencing an increase of more than 18%. This

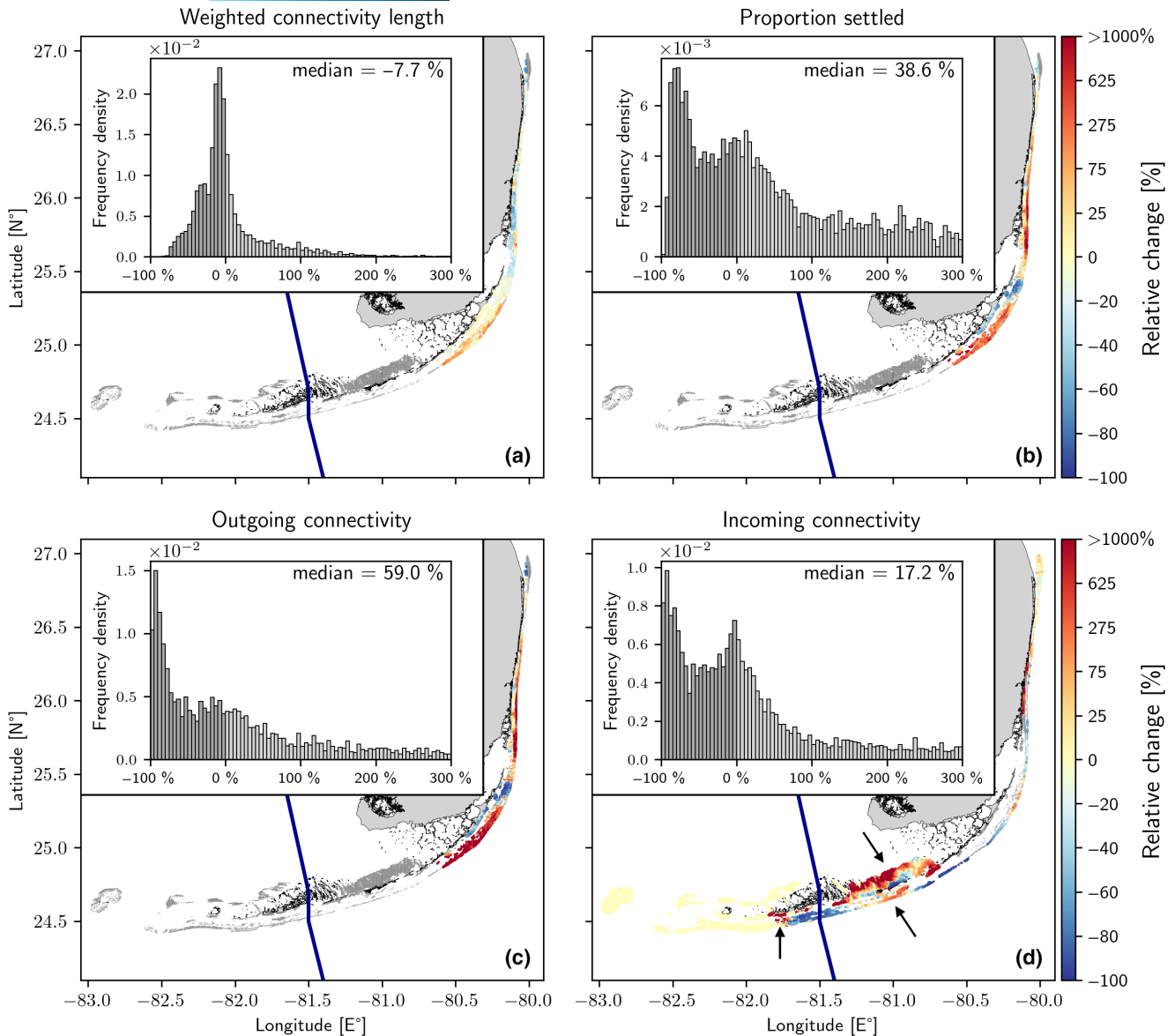


**FIGURE 4** Same as Figure 3 for disease dispersal. Note that the zero values in panel (d) west of the Lower Keys correspond to reefs for which there is no incoming connectivity both with and without Irma. The relative change is thus undefined and they are not considered in the frequency density histogram. Arrows in panel (d) highlight patches of susceptible reefs that experienced a surge in incoming disease connectivity following the passage of Irma.

means that genes carrying some advantageous features were able to spread more rapidly through the coral reef ecosystem, hence bolstering its resilience and adaptation.

More generally, our study illustrates the varying impacts a hurricane can have on connectivity on either side of its track. In the Northern Hemisphere, hurricanes rotate counterclockwise. Consequently, for a hurricane approaching perpendicular to the shore, the wind-driven flow will be directed toward the coast on the right side of the track and toward the sea on the left side. There will further be a wave-driven flow acceleration along the shore in the area where the hurricane track intersects the shoreline, which can reverse the direction of the main transport pathways. For barrier reefs like FCR or the Mesoamerican Reef, this results in shorter and stronger larval exchanges on the right side of the track. Conversely,

on the left side, there will be longer and weaker exchanges. In the Southern Hemisphere, hurricanes rotate clockwise and the opposite conclusions hold. While these general patterns are influenced by the specific topography of the reef system, they nonetheless suggest that reefs on the right side of the track (where hurricane winds are stronger) may benefit more from changes in larval connectivity patterns.

Despite its fleeting occurrence, Hurricane Irma strongly influenced larval transport pathways. In our hypothetical test case comparing two spawning events, one before and the other after the passage of the hurricane, it resulted in a more intense flushing of the larvae away from their source reef. This increase in larval dispersal is consistent with previous modeling studies showing a decrease in retention rates over reefs (Grimaldi et al., 2022) and an increase in the

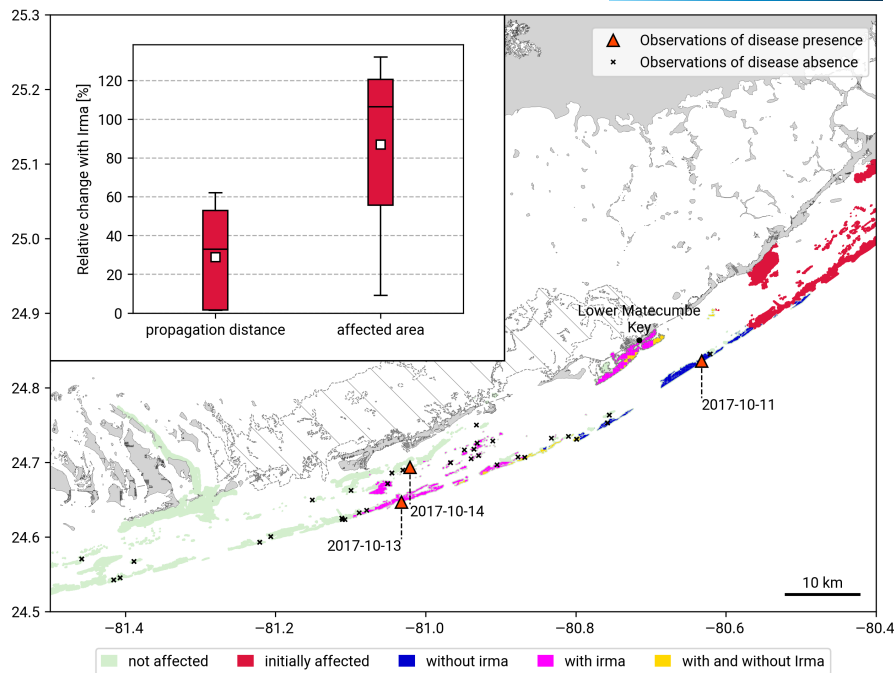


**FIGURE 5** Propagation of the disease simulated by the connectivity-based epidemiological model between September 1 and December 1, 2017 using the reference (dark blue) and hurricane (magenta) connectivity matrices. Reefs affected by stony coral tissue loss disease prior to September 1, 2017 are shown in red and fully susceptible reefs in green. Vaca Reef, which was filtered out of the connectivity matrices, is represented by a hashed white polygon. Observations of disease presence and absence between the landfall of Irma and December 1, 2017, respectively, shown by red triangles and black crosses. These observations were extracted from (i) Coral Reef Evaluation and Monitoring Project (CREMP; 2014–2017), (ii) CREMP Presence/Absence Data (CREMP P\_A; 2016–2017), (iii) Southeast Florida Coral Reef Evaluation and Monitoring Project (SECREMP; 2014–2017), (iv) Florida Reef Resilience Program Disturbance Response Monitoring (FRRP; 2014–2017), (v) Hurricane Irma Rapid Reef Assessment (IRMA; 2017), (vi) the Southeast Florida Action Network citizen science program (SEAFAN; 2014–2017), and (vii) the Southern Coral Disease Margin field effort (2017 and 2018). The upper left graph shows the relative change in the distance traveled by the disease front and the total affected area when accounting for Irma for different values of the model's infection threshold. The central lines of the boxes and the white square respectively indicate the median and mean of the relative change, the bottom and top of the boxes indicate the 25th and 75th percentiles, respectively, while the minimum and maximum of the relative change are indicated by the bottom and top whiskers. On average, the hurricane caused a 28.9% increase in disease propagation distance and an 87.0% increase in affected area, equivalent to about 25 days of disease propagation under fair weather conditions.

distance traveled by larvae (Radford et al., 2014) during cyclones. In the Lower Keys, modeled currents from Irma drove larvae offshore, where currents are stronger, and hence increased the distance they could be transported over while diminishing the proportion of larvae that eventually settled and the outgoing connectivity index. In that area, Irma promoted longer but also weaker connections, thereby potentially allowing longer-distance genetic mixing within FCR. From the Middle Keys and further north, Irma may have driven larvae inshore, hence promoting exchanges from outer-shelf to inner-shelf reefs in the Middle Keys, hence potentially fostering the recolonization of inner shelf reefs. Radford et al. (2014) found similar results when simulating hurricane-induced inshore and offshore transport on the Australian northwestern shelf. Their results showed eastward transport when the cyclone was south of the reefs, and westward transport when it was north of the reefs.

The overall decrease in incoming connectivity indicates that only a minority of reefs benefited from the alterations of larval dispersal pathways. In our test case, three regions—the inner-shelf Middle Keys, the Upper Keys, and reefs north of Biscayne Bay—experienced

the greatest enhancement of larval supply due to the hurricane, albeit at the expense of other areas. These regions likely enhanced their resilience and genetic diversity by receiving larvae from more distant reefs, while the majority of FCR experienced a decrease in incoming connectivity. This decrease is not surprising as the current distribution of coral colonies mirrors long-term connectivity patterns. Corals tend to thrive in areas with a robust larval supply. Therefore, a significant alteration of these established connectivity patterns during an extreme event would likely result in a reduction in larval supply for most reefs. However, such disruptions of the long-term connectivity patterns during extreme events could also result in larvae colonizing reefs where they would not be able to settle under fair weather conditions.

All disease connectivity indicators point toward Hurricane Irma acting as a superspreader event for SCTLD, thereby accelerating the epidemic's spread. Indeed, while the hurricane-induced shoreward flow in the northern part of FCR shortened the dispersal of disease agents, the reefs at the frontline of the SCTLD epidemic witnessed a combined increase in WCL, outgoing connectivity

index, and proportion settled. Consequently, our model suggests that Irma may have facilitated the successful settlement of the disease onto a larger number of susceptible reefs and potentially aided the disease's propagation over greater distances, particularly for pathogens originating from reefs at the epidemic's front-line. This result was further demonstrated by epidemiological simulations, suggesting that the impact of Irma was equivalent to about 25 days of disease propagation under fair weather conditions. This accelerated spread was due to the disease propagating through the reefs with an increased incoming connectivity under the effect of Irma. The location of the disease front on the right of the hurricane's track favored this enhanced transport as it allowed disease agents to be carried away by the strong westward alongshore current that developed offshore of the landfall location (Figure 2b). This hurricane's effect on disease agents dispersal would also apply to other waterborne threats to coral reefs such as pollutants, sediment plumes, and predatory species larvae (Pratchett et al., 2017).

Our findings are consistent with previous studies that have shown that hurricanes are a vector of species range expansion, particularly in the Caribbean and Gulf of Mexico, which are frequently impacted by hurricanes. For instance, Johnston and Purkis (2015) have linked the expansion patterns of the invasive lionfish from Florida to the Bahamas to hurricane frequency. They showed that hurricanes could have sufficiently disturbed the FC to allow lionfish larvae to be transported across the Florida Straits and reach the Bahamas, where they rapidly spread through the archipelago. Similarly, Kennedy et al. (2020) showed that hurricanes, and particularly Hurricane Irma, fostered Florida mangrove pole-ward range expansion by opening short windows of long-distance dispersal and hence accelerated the species range shift. Multiple marine species with dispersal-driven reproduction occurring within the hurricane season can therefore take advantage of these extreme weather events to homogenize their gene pool and colonize new areas.

As with any modeling study, it is important to acknowledge the assumptions underpinning the model. The 2D barotropic ocean model employed in this study is well-suited for shallow waters but not for the deep ocean. To address this, we coupled it with the 3D HYCOM model, enabling an indirect representation of baroclinic phenomena. However, while this coupling allowed us to accurately model small-scale flow features near reefs, it could not fully capture mesoscale eddies present between the outer shelf and the FC that can influence coral connectivity. Consequently, we might have overlooked the effects of the hurricane on the vertical structure of the FC (Ezer, 2018) and these recirculating eddies, potentially leading to underestimations or overestimations of changes in local retention and WCL in the outer shelf. Moreover, the wave-coupling model could be refined by considering the momentum loss due to surface wave action and heat exchanges between the ocean and the atmosphere. We also did not consider the impact of reduced asymmetry in hurricane wind and waves caused by the observed global slowdown of cyclone translation speed (Kossin, 2018). Slower hurricanes have

the potential to generate larger waves, which might amplify their impact on connectivity. Additionally, the pressure within the radius of maximum wind speed of Irma was modeled based on best track data, which contain inherent uncertainties (Torn & Snyder, 2012). However, the modeled pressure showed reasonable agreement with available observations (Dobbelaere, Curcic, et al., 2022).

Another limitation was the simplification of biological parameters for coral larvae, which could be enriched by considering the effect of decreased water quality post-hurricane on egg-production and post-settlement processes. For instance, reef burial by silty sediments after the passage of Irma was not considered, and may have made larval settlement impossible on some reefs. A possible increase in larval mortality due to increased turbulence during the passage of the hurricane was not considered either (Heyward & Negri, 2012). We also did not consider changes to these parameters due to rising ocean temperature and hence did not consider future climate connectivity patterns. Due to the coarse spatial resolution of available coral density observations, we only modeled potential coral connectivity. Hence, we further assumed that all reefs had the same *M. cavernosa* coral cover and did not account for habitat quality. Assuming a uniform coral cover could have overestimated the disease spread, as some reefs that served as stepping stones for the outbreak might have lacked enough susceptible corals to sustain the disease. Finally, for the sake of illustration, we considered two hypothetical three-day spawning events immediately preceding and following the hurricane's passage to better highlight changes attributable to the passage of the hurricane. We therefore did not consider any larvae spawned earlier. Our results are relatively insensitive to the precise timing of the spawning periods as the connectivity indicators obtained for coral larvae and disease agents are very similar despite the different release time windows for coral larvae and disease agents.

While the frequency of tropical cyclones is not projected to increase (Walsh et al., 2019), their intensity, rate of intensification, and duration are expected to rise (Bhatia et al., 2022). This has been exemplified by several Category 5-equivalent tropical cyclones such as Ian (Atlantic Ocean, September 2022), Freddy (South Indian Ocean, February–March 2023), and Mocha (North Indian Ocean, May 2023). Tropical cyclones may coincide with coral spawning seasons, thereby directly impacting the dispersal of coral larvae. By fostering long-distance dispersal, they can facilitate genetic mixing, which is particularly beneficial in promoting the spread of disease-adapted or warm-adapted genes. This latter aspect offers a glimmer of hope as tropical cyclones could help counterbalance the effect of warming ocean temperature on coral larval development. By increasing early larval mortality and reducing the time taken by larvae to settle (Heyward & Negri, 2010; Nozawa & Harrison, 2007), global warming is indeed expected to shorten larval dispersal patterns and hence reduce connectivity (Figueiredo et al., 2022). Despite the destruction and uncertainty they bring, major tropical cyclones therefore have the potential to maintain long-distance larval exchanges, hence possibly aiding coral reefs in adapting to climate change.

## AUTHOR CONTRIBUTIONS

**Thomas Dobbelaere:** Conceptualization; software; writing – review and editing. **Apolline Dekens:** Investigation; writing – original draft. **Antoine Saint-Amand:** Methodology; resources. **Lauranne Alaerts:** Methodology; resources; software. **Daniel M. Holstein:** Conceptualization; writing – review and editing. **Emmanuel Hanert:** Conceptualization; project administration; supervision; writing – review and editing.

## ACKNOWLEDGMENTS

Computational resources have been provided by the supercomputing facilities of the Université catholique de Louvain (CISM/UCLouvain) and the Consortium des Équipements de Calcul Intensif en Fédération Wallonie Bruxelles (CECI) funded by the Fonds de la Recherche Scientifique de Belgique (F.R.S.-FNRS) under convention 2.5020.11. Thomas Dobbelaere is a postdoctoral researcher supported by the *Fonds de la Recherche Scientifique de Belgique* (F.R.S.-FNRS).

## CONFLICT OF INTEREST STATEMENT

The authors declare no competing interests.

## DATA AVAILABILITY STATEMENT

The datasets generated during this study are available from Dryad at <https://doi.org/10.5061/dryad.0cfxpnw98>.

## CODE AVAILABILITY STATEMENT

The SLIM source code can be found at <https://git.immc.ucl.ac.be/slim/slim>.

## ORCID

Thomas Dobbelaere  <https://orcid.org/0000-0001-9975-8695>

Daniel M. Holstein  <https://orcid.org/0000-0002-9933-833X>

## REFERENCES

- Aijaz, S., Ghantous, M., Babanin, A. V., Ginis, I., Thomas, B., & Wake, G. (2017). Nonbreaking wave-induced mixing in upper ocean during tropical cyclones using coupled hurricane-ocean-wave modeling. *Journal of Geophysical Research, Oceans*, *122*, 3939–3963. <https://doi.org/10.1002/2016JC012219>
- Allahdadi, M. N., & Li, C. (2017). Effect of stratification on current hydrodynamics over Louisiana shelf during hurricane Katrina. *Water Science and Engineering*, *10*, 154–165. <https://doi.org/10.1016/j.wse.2017.03.012>
- Alvarez-Filip, L., González-Barrios, F. J., Pérez-Cervantes, E., Molina-Hernández, A., & Estrada-Saldivar, N. (2022). Stony coral tissue loss disease decimated Caribbean coral populations and reshaped reef functionality. *Communications Biology*, *5*, 440. <https://doi.org/10.1038/s42003-022-03398-6>
- Aronson, R. B., Precht, W. F., Aronson, R. B., & Precht, W. F. (2001). White-band disease and the changing face of Caribbean coral reefs. *Hydrobiologia*, *460*, 25–38. <https://doi.org/10.1023/A:1013103928980>
- Banks, K. W., Riegl, B. M., Richards, V. P., Walker, B. K., Helme, K. P., Jordan, L. K. B., Phipps, J., Shivji, M. S., Speiler, R. E., & Dodge, R. E. (2008). The reef tract of continental Southeast Florida (Miami-Dade, Broward and Palm Beach Counties, USA). In B. M. Riegl & R. E. Dodge (Eds.), *Coral reefs of the USA* (pp. 175–220). Springer. [https://doi.org/10.1007/978-1-4020-6847-8\\_5](https://doi.org/10.1007/978-1-4020-6847-8_5)
- Bhatia, K., Baker, A., Yang, W., Vecchi, G., Knutson, T., Murakami, H., Kossin, J., Hodges, K., Dixon, K., Bronselaer, B., & Whitlock, C. (2022). A potential explanation for the global increase in tropical cyclone rapid intensification. *Nature Communications*, *13*, 6626.
- Bhatia, K. T., Vecchi, G. A., Knutson, T. R., Murakami, H., Kossin, J., Dixon, K. W., & Whitlock, C. E. (2019). Recent increases in tropical cyclone intensification rates. *Nature Communications*, *10*, 635. <https://doi.org/10.1038/s41467-019-08471-z>
- Bonin, M. C., Almany, G. R., & Jones, G. P. (2011). Contrasting effects of habitat loss and fragmentation on coral-associated reef fishes. *Ecology*, *92*, 1503–1512.
- Booi, N., Ris, R. C., & Holthuijsen, L. H. (1999). A third-generation wave model for coastal regions: 1. Model description and validation. *Journal of Geophysical Research, Oceans*, *104*, 7649–7666. <https://doi.org/10.1029/98JC02622>
- Bright, A., Peterson, A., Ladd, M., & Williams, D. (2021). *Quicklook report: Coral spawning 2020: Activities and observations*. NOAA. <https://doi.org/10.25923/y12y-7850>
- Bruno, J. F., Petes, L. E., Harvell, C. D., & Hettinger, A. (2003). Nutrient enrichment can increase the severity of coral diseases. *Ecology Letters*, *6*, 1056–1061. <https://doi.org/10.1046/j.1461-0248.2003.00544.x>
- Cangialosi, J. P., Latta, A. S., & Berg, R. (2018). *National hurricane center tropical cyclone report: Hurricane Irma (30 August–12 September 2017)*. Technical Report, National Oceanic and Atmospheric Administration and National Hurricane Center.
- Carrigan, A. D., & Puotinen, M. (2014). Tropical cyclone cooling combats region-wide coral bleaching. *Global Change Biology*, *20*, 1604–1613.
- Carter, A. L., Gilchrist, H., Dexter, K. G., Gardner, C. J., Gough, C., Roccliffe, S., & Wilson, A. M. W. (2022). Cyclone impacts on coral reef communities in Southwest Madagascar. *Frontiers in Marine Science*, *9*, 753325. <https://doi.org/10.3389/fmars.2022.753325>
- Chassignet, E. P., Hurlburt, H. E., Smedstad, O. M., Halliwell, G. R., & Bleck, R. (2007). The HYCOM (Hybrid Coordinate Ocean Model) data assimilative system. *Journal of Marine Systems*, *65*, 60–83. <https://doi.org/10.1016/j.jmarsys.2005.09.016>
- De'ath, G., Fabricius, K. E., Sweatman, H., & Puotinen, M. (2012). The 27-year decline of coral cover on the Great Barrier Reef and its causes. *Proceedings of the National Academy of Sciences of the United States of America*, *109*, 17995–17999. <https://doi.org/10.1073/pnas.1208909109>
- Dobbelaere, T., Curcic, M., Le Hénaff, M., & Hanert, E. (2022). Impacts of Hurricane Irma (2017) on wave-induced ocean transport processes. *Ocean Modelling*, *171*, 101947. <https://doi.org/10.1016/j.ocemod.2022.101947>
- Dobbelaere, T., Holstein, D. M., Muller, E. M., Gramer, L. J., McEachron, L., Williams, S. D., & Hanert, E. (2022). Connecting the dots: Transmission of stony coral tissue loss disease from the Marquesas to the Dry Tortugas. *Frontiers in Marine Science*, *9*, 778938.
- Dobbelaere, T., Muller, E. M., Gramer, L. J., Holstein, D. M., & Hanert, E. (2020). Coupled epidemio-hydrodynamic modeling to understand the spread of a deadly coral disease in Florida. *Frontiers in Marine Science*, *7*, 1016.
- Donahue, S., Acosta, A., Akins, L., Ault, J., & Cox, C. (2008). The state of coral reef ecosystems of the Florida Keys. In J. E. Waddell & A. M. Clarke (Eds.), *The state of coral reef ecosystems of the United States and Pacific freely associated states: 2008* (pp. 161–187). NOAA.
- Dove, S. G., Brown, K. T., Van Den Heuvel, A., Chai, A., & Hoegh-Guldberg, O. (2020). Ocean warming and acidification uncouple calcification from calcifier biomass which accelerates coral reef decline. *Communications Earth & Environment*, *1*, 1–9. <https://doi.org/10.1038/s43247-020-00054-x>
- Eddy, T. D., Lam, V. W. Y., Reygondeau, G., Cisneros-Montemayor, A. M., Greer, K., Palomares, M. L. D., Bruno, J. F., Ota, Y., & Cheung, W.

- W. L. (2021). Global decline in capacity of coral reefs to provide ecosystem services. *One Earth*, 4, 1278–1285. <https://doi.org/10.1016/j.oneear.2021.08.016>
- Egbert, G. D., & Erofeeva, S. Y. (2002). Efficient inverse modeling of barotropic ocean tides. *Journal of Atmospheric and Oceanic Technology*, 19, 183–204. [https://doi.org/10.1175/1520-0426\(2002\)019<0183:EIMOBO>2.0.CO;2](https://doi.org/10.1175/1520-0426(2002)019<0183:EIMOBO>2.0.CO;2)
- Elliff, C. I., & Silva, I. R. (2017). Coral reefs as the first line of defense: Shoreline protection in face of climate change. *Marine Environmental Research*, 127, 148–154. <https://doi.org/10.1016/j.marenvres.2017.03.007>
- Ertfemeijer, P. L. A., Riegl, B., Hoeksema, B. W., & Todd, P. A. (2012). Environmental impacts of dredging and other sediment disturbances on corals: A review. *Marine Pollution Bulletin*, 64, 1737–1765. <https://doi.org/10.1016/j.marpolbul.2012.05.008>
- Ezer, T. (2018). On the interaction between a hurricane, the Gulf stream and coastal sea level. *Ocean Dynamics*, 68, 1259–1272.
- Ferrario, F., Beck, M. W., Storlazzi, C. D., Micheli, F., Shepard, C. C., & Airoidi, L. (2014). The effectiveness of coral reefs for coastal hazard risk reduction and adaptation. *Nature Communications*, 5, 3794. <https://doi.org/10.1038/ncomms4794>
- Figueiredo, J., Thomas, C. J., Deleersnijder, E., Lambrechts, J., Baird, A. H., Connolly, S. R., & Hanert, E. (2022). Global warming decreases connectivity among coral populations. *Nature Climate Change*, 12, 83–87. <https://doi.org/10.1038/s41558-021-01248-7>
- Finkl, C. W., & Andrews, J. L. (2008). Shelf geomorphology along the Southeast Florida Atlantic continental platform: Barrier coral reefs, nearshore bedrock, and morphosedimentary features. *Journal of Coastal Research*, 244, 2008–2849. <https://doi.org/10.2112/08A-0001.1>
- Florida Fish and Wildlife Conservation Commission-Fish and Wildlife Research Institute. (2017). *Tract map v2.0*. [https://ocean.floridamarine.org/IntegratedReefMap/Docs/Metadata\\_UnifiedFloridaCoralReefMap\\_v20.html](https://ocean.floridamarine.org/IntegratedReefMap/Docs/Metadata_UnifiedFloridaCoralReefMap_v20.html)
- Frys, C., Saint-Amand, A., le Hénaff, M., Figueiredo, J., Kuba, A., Walker, B., Lambrechts, J., Vallaeys, V., Vincent, D., & Hanert, E. (2020). Fine-scale coral connectivity pathways in the Florida reef tract: Implications for conservation and restoration. *Frontiers in Marine Science*, 7, 312. <https://doi.org/10.3389/fmars.2020.00312>
- Grimaldi, C. M., Lowe, R. J., Benthuisen, J. A., Cuttler, M. V. W., Green, R. H., Radford, B., Ryan, N., & Gilmour, J. (2022). Hydrodynamic drivers of fine-scale connectivity within a coral reef atoll. *Limnology and Oceanography*, 67, 2204–2217.
- Grove, L. J. W., Grove, L. J. W., Blondeau, J., Cain, E., Davis, I. M., Edwards, K. F., Groves, S. H., Hile, S. D., Langwiser, C., Siceloff, L., Swanson, D. W., Towle, E. K., Viehman, T. S., & Williams, B. (2022). *National Coral Reef Monitoring Program, biological monitoring summary – Florida: 2020–2021*.
- Hagman, D. K., Gittings, S. R., & Deslarzes, K. J. (1998). Timing, species participation, and environmental factors influencing annual mass spawning at the Flower Garden Banks (Northwest Gulf of Mexico). *Gulf of Mexico Science*, 16, 6.
- Her, Y. G., Smyth, A., Fletcher, P., Bassil, E., Stingl, U., Brym, Z., & Qui, J. (2021). *Hurricane impacts on Florida's agriculture and natural resources*. <https://edis.ifas.ufl.edu/publication/AE528>
- Hersbach, H., Bell, B., Berrisford, P., Hirahara, S., Horányi, A., Muñoz-Sabater, J., Nicolas, J., Peubey, C., Radu, R., Schepers, D., Simmons, A., Soci, C., Abdalla, S., Abellan, X., Balsamo, G., Bechtold, P., Biavati, G., Bidlot, J., Bonavita, M., ... Thépaut, J. N. (2020). The ERA5 global reanalysis. *Quarterly Journal of the Royal Meteorological Society*, 146, 1999–2049.
- Heyward, A., & Negri, A. (2010). Plasticity of larval pre-competency in response to temperature: Observations on multiple broadcast spawning coral species. *Coral Reefs*, 29, 631–636.
- Heyward, A., & Negri, A. (2012). Turbulence, cleavage, and the naked embryo: A case for coral clones. *Science*, 335, 1064.
- Hoegh-Guldberg, O., Pendleton, L., & Kaup, A. (2019). People and the changing nature of coral reefs. *Regional Studies in Marine Science*, 30, 100699. <https://doi.org/10.1016/j.rmsa.2019.100699>
- Hoffmeister, J. E., & Multer, H. G. (1968). Geology and origin of the Florida Keys. *GSA Bulletin*, 79, 1487–1502. [https://doi.org/10.1130/0016-7606\(1968\)79\[1487:GAOOFJ\]2.0.CO;2](https://doi.org/10.1130/0016-7606(1968)79[1487:GAOOFJ]2.0.CO;2)
- Johnston, M. W., & Purkis, S. J. (2015). Hurricanes accelerated the Florida–Bahamas lionfish invasion. *Global Change Biology*, 21, 2249–2260.
- Jones, R., Ricardo, G. F., & Negri, A. P. (2015). Effects of sediments on the reproductive cycle of corals. *Marine Pollution Bulletin*, 100, 13–33. <https://doi.org/10.1016/j.marpolbul.2015.08.021>
- Kennedy, J. P., Dangremond, E. M., Hayes, M. A., Preziosi, R. F., Rowntree, J. K., & Feller, I. C. (2020). Hurricanes overcome migration lag and shape intraspecific genetic variation beyond a poleward mangrove range limit. *Molecular Ecology*, 29, 2583–2597.
- King, S., Saint-Amand, A., Walker, B. K., Hanert, E., & Figueiredo, J. (2023). Larval dispersal patterns and connectivity of *Acropora* on Florida's Coral Reef and its implications for restoration. *Frontiers in Marine Science*, 9, 1038463.
- Kline, D. I., & Vollmer, S. V. (2011). White band disease (type I) of endangered Caribbean Acroporid corals is caused by pathogenic bacteria. *Scientific Reports*, 1, 7. <https://doi.org/10.1038/srep00007>
- Knutson, T., Camargo, S. J., Chan, J. C. L., Emanuel, K., Ho, C. H., Kossin, J., Mohapatra, M., Satoh, M., Sugi, M., Walsh, K., & Wu, L. (2020). Tropical cyclones and climate change assessment: Part II: Projected response to anthropogenic warming. *Bulletin of the American Meteorological Society*, 101, E303–E322. <https://doi.org/10.1175/BAMS-D-18-0194.1>
- Kossin, J. P. (2018). A global slowdown of tropical-cyclone translation speed. *Nature*, 558, 104–107.
- Kourafalou, V. H., & Kang, H. (2012). Florida current meandering and evolution of cyclonic eddies along the Florida Keys Reef Tract: Are they interconnected? *Journal of Geophysical Research, Oceans*, 117, 5028. <https://doi.org/10.1029/2011JC007383>
- Kuba, A. (2016). *Transgenerational effects of thermal stress: Impacts on and beyond coral reproduction*. NSUWorks.
- Kundu, P. K. (1976). Ekman veering observed near the ocean bottom. *Journal of Physical Oceanography*, 6, 238–242.
- Lambrechts, J., Hanert, E., Deleersnijder, E., Bernard, P. E., Legat, V., Remacle, J. F., & Wolanski, E. (2008). A multi-scale model of the hydrodynamics of the whole Great Barrier Reef. *Estuarine, Coastal and Shelf Science*, 79, 143–151.
- Le, H.-A., Lambrechts, J., Ortleb, S., Gratiot, N., Deleersnijder, E. L. C., & Soares-Frazaõ, S. (2020). An implicit wetting–drying algorithm for the discontinuous Galerkin method: Application to the Tonle Sap, Mekong River Basin. *Environmental Fluid Mechanics*, 20, 923–951. <https://doi.org/10.1007/s10652-019-09732-7>
- Lee, T. N., Clarke, M. E., Williams, E., Szmant, A. F., & Berger, T. (1994). Evolution of the Tortugas gyre and its influence on recruitment in the Florida Keys. *Bulletin of Marine Science*, 54, 621–646.
- Lee, T. N., & Smith, N. (2002). Volume transport variability through the Florida Keys tidal channels. *Continental Shelf Research*, 22, 1361–1377. [https://doi.org/10.1016/S0278-4343\(02\)00003-1](https://doi.org/10.1016/S0278-4343(02)00003-1)
- Leipper, D. F. (1970). A sequence of current patterns in the Gulf of Mexico. *Journal of Geophysical Research*, 75, 637–657. <https://doi.org/10.1029/JC075i003p00637>
- Limouzy-Paris, C. B., Graber, H. C., Jones, D. L., Röpke, A. W., & Richards, W. J. (1997). Translocation of larval coral reef fishes via sub-mesoscale spin-off eddies from the Florida current. *Bulletin of Marine Science*, 60, 966–983.
- Liu, Y., Weisberg, R. H., & Zheng, L. (2020). Impacts of hurricane Irma on the circulation and transport in Florida Bay and the Charlotte Harbor estuary. *Estuaries and Coasts*, 43, 1194–1216.
- Lyons, M. B., Murray, N. J., Kennedy, E. V., Kovacs, E. M., Castro-Sanguino, C., Phinn, S. R., Acevedo, R. B., Alvarez, A. O., Say, C.,

- Tudman, P., Markey, K., Roe, M., Canto, R. F., Fox, H. E., Bambic, B., Lieb, Z., Asner, G. P., Martin, P. M., Knapp, D. E., ... Roelfsema, C. M. (2024). New global area estimates for coral reefs from high-resolution mapping. *Cell Reports Sustainability*, 1, 100015.
- Malmstadt, J., Scheitlin, K., & Elsner, J. (2009). Florida hurricanes and damage costs. *Southeastern Geographer*, 49, 108–131. <https://doi.org/10.1353/sgo.0.0045>
- Manzello, D. P., Brandt, M., Smith, T. B., Lirman, D., Hendee, J. C., & Nemeth, R. S. (2007). Hurricanes benefit bleached corals. *Proceedings of the National Academy of Sciences of the United States of America*, 104, 12035–12039. <https://doi.org/10.1073/pnas.0701194104>
- Moberg, F., & Folke, C. (1999). Ecological goods and services of coral reef ecosystems. *Ecological Economics*, 29, 215–233. [https://doi.org/10.1016/S0921-8009\(99\)00009-9](https://doi.org/10.1016/S0921-8009(99)00009-9)
- Monroy, P., Rossi, V., Ser-Giacomi, E., Lopez, C., & Hernandez-Garcia, E. (2017). Sensitivity and robustness of larval connectivity diagnostics obtained from Lagrangian flow networks. *ICES Journal of Marine Science*, 74, 1763–1779. <https://doi.org/10.1093/icesjms/fsw235>
- Muller, E. M., Bartels, E., & Baums, I. B. (2018). Bleaching causes loss of disease resistance within the threatened coral species *Acropora cervicornis*. *eLife*, 7, e35066.
- Muller, E. M., Sartor, C., Alcaraz, N. I., & Van Woesik, R. (2020). Spatial epidemiology of the stony-coral-tissue-loss disease in Florida. *Frontiers in Marine Science*, 7, 163.
- Muller, E. M., & van Woesik, R. (2012). Caribbean coral diseases: Primary transmission or secondary infection? *Global Change Biology*, 18, 3529–3535.
- Murphy, B. S. (2014). PyKrig: Development of a kriging toolkit for Python. *AGU fall meeting abstracts*. H51K-0753.
- Neely, K. (2018). *Surveying the Florida Keys southern coral disease boundary*. Final summary report.
- Neumann, C. J. (1999). *Tropical cyclones of the North Atlantic ocean, 1871–1998*. <https://repository.library.noaa.gov/view/noaa/1086>
- NOAA. (2018a). *Costliest U.S. tropical cyclones tables updated*. <https://www.nhc.noaa.gov/news/UpdatedCostliest.pdf>
- NOAA. (2018b). *Stony coral tissue loss disease case definition*. <https://nmsfloridakeys.blob.core.windows.net/floridakeys-prod/media/docs/20181002-stony-coral-tissue-loss-disease-case-definition.pdf>
- NOAA. (2020). *NOAA strategy for stony coral tissue loss disease response and prevention*. [https://www.coris.noaa.gov/activities/sctId\\_strategy/welcome.html](https://www.coris.noaa.gov/activities/sctId_strategy/welcome.html)
- NOAA. (2022). *NOAA and partners assess reef, aid recovery following Hurricane Irma*. <https://sanctuaries.noaa.gov/news/jan18/noaa-and-partners-assess-reef-aid-recovery-following-irma.html>
- Nozawa, Y., & Harrison, P. L. (2007). Effects of elevated temperature on larval settlement and post-settlement survival in scleractinian corals, *Acropora solitaryensis* and *Favites chinensis*. *Marine Biology*, 152, 1181–1185.
- Oey, L.-Y., Ezer, T., Wang, D.-P., Yin, X.-Q., & Fan, S.-J. (2007). Hurricane-induced motions and interaction with ocean currents. *Continental Shelf Research*, 27, 1249–1263. <https://doi.org/10.1016/j.csr.2007.01.008>
- Porter, J. W., & Meier, O. W. (1992). Quantification of loss and change in Floridian reef coral populations. *Integrative and Comparative Biology*, 32, 625–640. <https://doi.org/10.1093/icb/32.6.625>
- Powell, M. D., Houston, S. H., Amat, L. R., & Morisseau-Leroy, N. (1998). The HRD real-time hurricane wind analysis system. *Journal of Wind Engineering and Industrial Aerodynamics*, 77–78, 53–64. [https://doi.org/10.1016/S0167-6105\(98\)00131-7](https://doi.org/10.1016/S0167-6105(98)00131-7)
- Pratchett, M. S., Caballes, C. F., Wilmes, J. C., Matthews, S., Mellin, C., Sweatman, H. P., Nadler, L. E., Brodie, J., Thompson, C. A., Hoey, J., & Bos, A. R. (2017). Thirty years of research on crown-of-thorns starfish (1986–2016): Scientific advances and emerging opportunities. *Diversity*, 9, 41.
- Precht, W. F., Gintert, B. E., Robbart, M. L., Fura, R., & van Woesik, R. (2016). Unprecedented disease-related coral mortality in south-eastern Florida. *Scientific Reports*, 6, 31374. <https://doi.org/10.1038/srep31374>
- Radford, B., Babcock, R., Van Niel, K., & Done, T. (2014). Are cyclones agents for connectivity between reefs? *Journal of Biogeography*, 41, 1367–1378.
- Rogers, A., Blanchard, J. L., & Mumby, P. J. (2014). Vulnerability of coral reef fisheries to a loss of structural complexity. *Current Biology*, 24, 1000–1005. <https://doi.org/10.1016/j.cub.2014.03.026>
- Ruzicka, R. R., Colella, M. A., Porter, J. W., Morrison, J. M., Kidney, J. A., Brinkhuis, V., Lunz, K. S., Macaulay, K. A., Bartlett, L. A., Meyers, M. K., & Colee, J. (2013). Temporal changes in benthic assemblages on Florida Keys reefs 11 years after the 1997/1998 El Niño. *Marine Ecology Progress Series*, 489, 125–141. <https://doi.org/10.3354/meps10427>
- Scoffin, T. P. (1993). The geological effects of hurricanes on coral reefs and the interpretation of storm deposits. *Coral Reefs*, 12, 203–221. <https://doi.org/10.1007/BF00334480>
- Shulman, M. J., & Bermingham, E. (1995). Early life histories, ocean currents, and the population genetics of Caribbean reef fishes. *Evolution*, 49, 897–910. <https://doi.org/10.1111/j.1558-5646.1995.tb02325.x>
- Sponaugle, S., & Lee, T. (2007). Patterns and processes of larval fish supply to the coral reefs of the upper Florida keys. *Marine Ecology Progress Series*, 331, 85–100. <https://doi.org/10.3354/meps331085>
- Thomas, C. J., Lambrechts, J., Wolanski, E., Traag, V. A., Blondel, V. D., Deleersnijder, E., & Hanert, E. (2014). Numerical modelling and graph theory tools to study ecological connectivity in the great barrier reef. *Ecological Modelling*, 272, 160–174. <https://doi.org/10.1016/j.ecolmodel.2013.10.002>
- Torn, R. D., & Snyder, C. (2012). Uncertainty of tropical cyclone best-track information. *Weather and Forecasting*, 27, 715–729.
- Varlas, G., Vervatis, V., Spyrou, C., Papadopoulou, E., & Katsafados, P. (2020). Investigating the impact of atmosphere-wave-ocean interactions on a Mediterranean tropical-like cyclone. *Ocean Modelling*, 153, 101675. <https://doi.org/10.1016/j.ocemod.2020.101675>
- Viehman, S., Gittings, S., Groves, S., Moore, J., Moore, T., & Stein, J. (2018). *NCCOS assessment: Coral disturbance response monitoring (DRM) along the Florida reef tract following hurricane Irma from 2017-10-09 to 2017-10-18 (NCEI accession 0179071)*. NOAA National Centers for Environmental Information. <https://doi.org/10.25921/sscd-6h41>
- Vukovich, F. M. (1988). Loop current boundary variations. *Journal of Geophysical Research, Oceans*, 93, 15585–15591. <https://doi.org/10.1029/JC093iC12p15585>
- Walsh, K. J., Camargo, S. J., Knutson, T. R., Kossin, J., Lee, T.-C., Murakami, H., & Patricola, C. (2019). Tropical cyclones and climate change. *Tropical Cyclone Research and Review*, 8, 240–250.
- Xian, S., Feng, K., Lin, N., Marsooli, R., & Hatzikyriakou, A. (2018). Brief communication: Rapid assessment of damaged residential buildings in the Florida Keys after Hurricane Irma. *Natural Hazards and Earth System Sciences*, 18, 2041–2045. <https://doi.org/10.5194/nhess-18-2041-2018>

**How to cite this article:** Dobbelaere, T., Dekens, A., Saint-Amand, A., Alaerts, L., Holstein, D. M., & Hanert, E. (2024). Hurricanes enhance coral connectivity but also superspread coral diseases. *Global Change Biology*, 30, e17382. <https://doi.org/10.1111/gcb.17382>

## APPENDIX

## Model validation

The simulated currents velocity was validated against depth-averaged ADCP measurements at University of South Florida's mooring stations C10, C12, and C13 available from NOAA's National Data Buoy Center (Figure A1). Station C10 is located on the 25m isobath, while stations C12 and C13 are located on the 50m isobath. As in Liu et al. (2020), we performed the vector correlation analysis of Kundu (1976) to compare modeled and observed

current velocity vectors. This analysis was performed for every simulated month but is only shown for September 2017 (Figure A1). Overall, there is a good agreement between model results and observations, both in terms of currents amplitude and direction. The intensification of the ocean currents during the passage of Irma is particularly visible. Correlation coefficients between simulated and observed depth-averaged currents during this month were 0.782, 0.748, and 0.796 at stations C10, C12, and C13 respectively, with average veering angles below  $10^\circ$ , which is similar to the results of Liu et al. (2020).

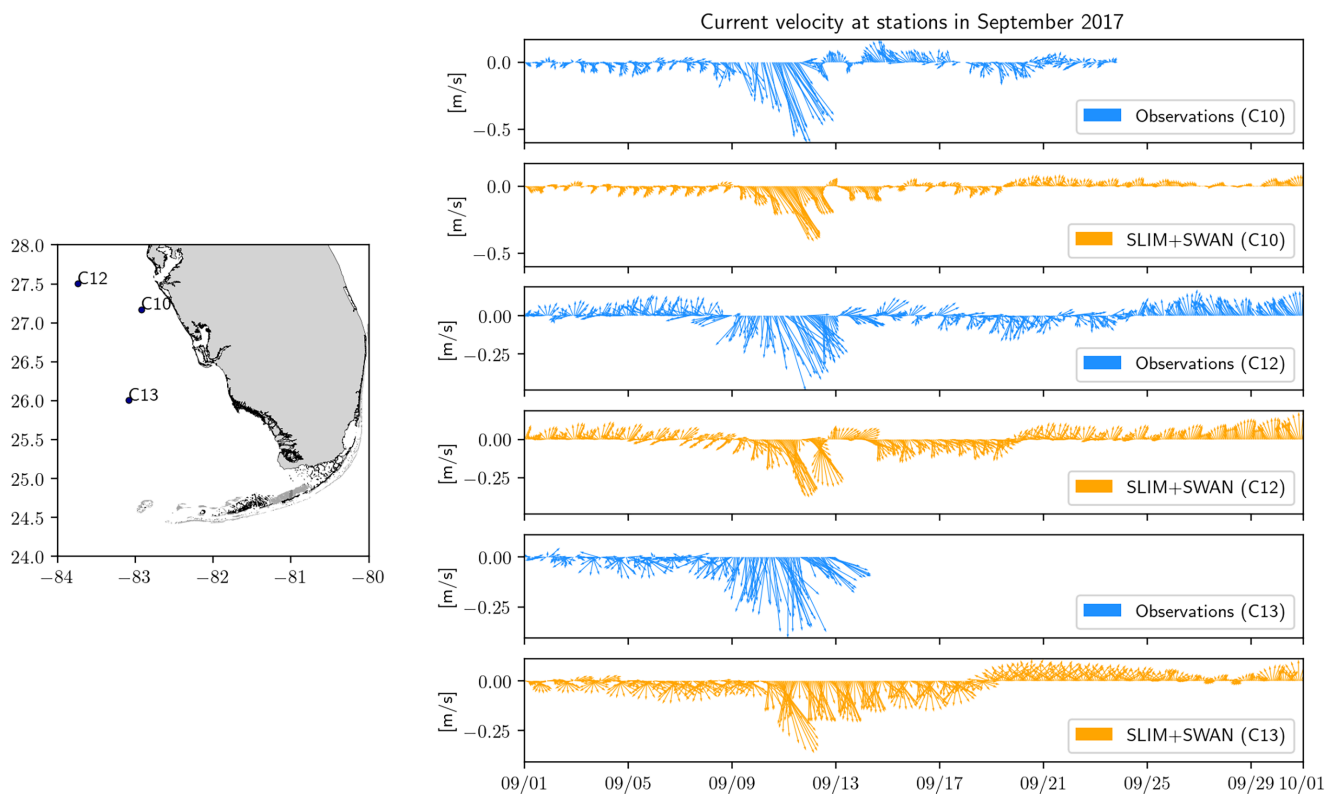


FIGURE A1 Validation of model outputs against ADCP current velocity measurements in September 2017.